Rapid Communications

Spectroscopic signatures of spin-orbit coupling and free excitons in individual suspended carbon nanotubes

Morgane Gandil,[1,2] Kazunari Matsuda,[3] Brahim Lounis,[1,2,*] and Philippe Tamarat[1,2,†]
[1]*Université Bordeaux, LP2N, F-33405 Talence, France*
[2]*Institut d'Optique & CNRS, LP2N, F-33405 Talence, France*
[3]*Institute of Advanced Energy, Kyoto University Gokasho, Uji, Kyoto 611-0011, Japan*

(Received 19 May 2019; published 26 August 2019)

We investigate the intrinsic magneto-optical properties of suspended single-walled carbon nanotubes of various chiralities, using a combination of spectrally and time-resolved spectroscopy of individual nanotubes at low temperature. This study elucidates the population and relaxation dynamics of the lowest-energy bright and dark singlet excitons that are mixed with the Aharonov-Bohm effect. The high-quality emission spectra reveal the residual oscillator strength of the dark exciton in zero field, as an optical signature of spin-orbit coupling. They also unveil an asymmetry in the bright exciton recombination line, attributed to the free nature of excitons in these unperturbed nanotubes.

DOI: 10.1103/PhysRevB.100.081411

Single-walled carbon nanotubes (SWCNTs) display a wide range of optical resonances [1,2] for optoelectronic device applications and fundamental studies of the light-matter interaction in one-dimensional nanostructures [3]. Their optical excitation leads to the formation of strongly bound electron-hole pairs known as excitons with exciton binding energies as high as a few hundred meV [4,5], due to weakly screened Coulomb interactions between charge carriers. Despite considerable theoretical and experimental efforts, the physics of the band-edge exciton fine structure, whose recombination is at the origin of the emission, has not been completely elucidated.

In semiconducting SWCNTs, there are two equivalent valleys (K and K') in momentum space having opposite helicities around the tube axis. Short-range Coulomb interactions cause intervalley mixing as well as singlet-triplet splitting, giving rise to an exciton fine structure consisting of 16 exciton states, with 12 spin-triplet states that are not expected to contribute to the photoluminescence (PL) and four spin-singlet states [6–8]. Among the singlet states, the two highest-energy degenerate states, called K-momentum excitons, have large center-of-mass momenta and thus cannot couple directly to photons [9]. The second lowest-energy state with odd parity and with zero momentum can recombine radiatively (bright exciton), while the ground exciton state with even parity and zero momentum is dipole forbidden (dark exciton) [10]. Under magnetic fields applied along the SWCNT axis, breaking of the time-reversal symmetry by the Aharonov-Bohm effect lifts the valley degeneracy and produces a transfer of oscillator strength from the bright exciton state to the dark [8,11,12]. Spectral signatures of such magnetic brightening of the lowest-energy exciton have been reported in the PL spectra of SWCNT ensembles [13,14] as well as single SWCNTs [10,15,16] at low temperature. Yet, the spectral fingerprint of the fine structure remains largely unexplored, such as the shapes and relative weights of the exciton recombination lines with and without magnetic field. Moreover, in the absence of the study of the PL decay of single SWCNTs under magnetic fields, little is known about how bright and dark states are populated after light absorption and how they thermally mix and relax afterwards. Here, we combine spectrally and time-resolved magneto-optical spectroscopy of single suspended SWCNTs to provide a thorough understanding of the photophysical properties of the band-edge exciton fine structure in these one-dimensional model nano-objects. These low-temperature spectroscopic investigations enable a robust determination of the dark and bright exciton populations and relaxation dynamics together with their magnetic field dependence. The quality of the PL spectra recorded with our experimental setup also unveils a residual oscillator strength of the dark exciton in zero magnetic field, whose origin is attributed to spin-orbit coupling. Strikingly, an asymmetry in the bright exciton PL lines with a blueshifted tail is evidenced for SWCNTs regardless of their chirality. It is interpreted as a signature of the free nature of one-dimensional excitons in these SWCNTs with reduced environmental perturbations.

The studied SWCNTs are synthesized on Si substrates, using an alcohol catalytic chemical vapor deposition method [17], and suspended over lithographed trenches of 0.5 μm in width and depth. Single nanotube measurements are performed with a home-built confocal optical microscope, using a 0.95 numerical aperture objective that is inserted in a magnetic helium cryostat together with the sample and a piezoscanner. The objective axis is perpendicular to the magnetic field, allowing magneto-optical studies in the Voigt configuration. The luminescence is filtered from the scattered excitation light and sent to a single-photon-counting superconducting device (temporal resolution 50 ps) and a spectrometer.

*brahim.lounis@u-bordeaux.fr
†philippe.tamarat@u-bordeaux.fr

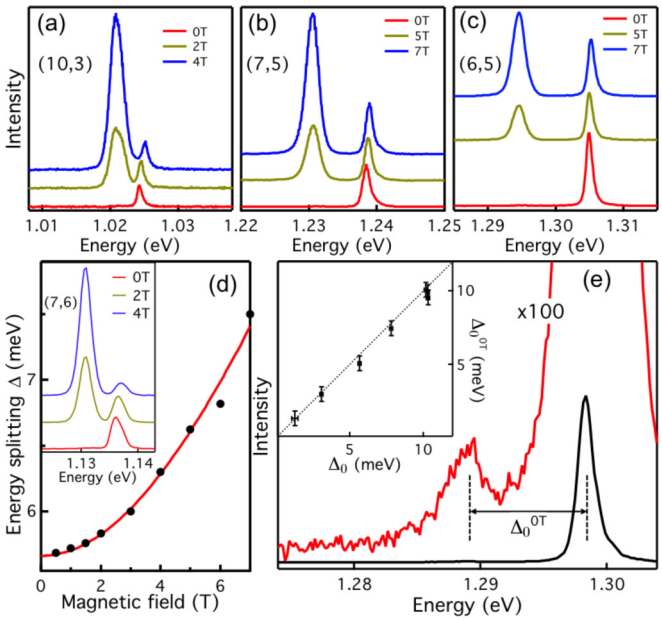

FIG. 1. (a)–(c) PL spectra of single SWCNTs with different chiralities excited on the S_{22} transition at weak continuous wave laser intensities ($\sim$1 kW cm^{-2}), under various magnetic fields and at 5 K. (d) Evolution of the energy splitting Δ with magnetic field for a (7,6) SWNT whose spectra are displayed in the inset. The red curve is a fit with $\Delta(B)$, yielding $\Delta_0 = 5.7$ meV and $w = 0.68$ meV T^{-1}. (e) Zero-field PL spectrum of a (6,5) SWCNT displayed on two different intensity scales. The low-energy peak is redshifted by Δ_0^{0T}, which matches the zero-field splitting Δ_0. The inset displays the correlation between Δ_0^{0T} and Δ_0 for SWCNTs of different chiralities.

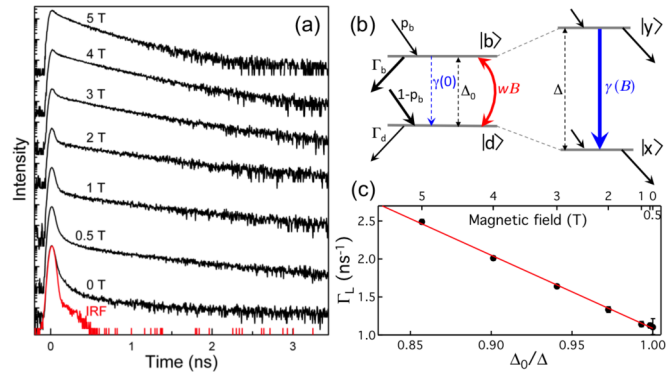

FIG. 2. (a) PL decay of a (7,6) SWCNT excited on the S_{22} transition under various magnetic fields at 4 K. The red curve represents the instrument response function. (b) Relaxation scheme within the two-level system in zero field and under magnetic field. (c) Relaxation rate of the long decay component as a function of Δ_0/Δ directly obtained from the PL spectra. The linear fit (red line) yields $\Gamma_d = 1.1$ ns^{-1} and $\Gamma_b = 20$ ns^{-1}.

Figures 1(a)–1(d) exemplify PL spectra of single SWCNTs with different chiralities at low temperature and under various magnetic fields. The spectra essentially exhibit a single peak in zero field, while a new line emerges with increasing magnetic fields and dominates the PL spectrum at 7 T. As reported in previous works [10,13,14,16], this magnetic brightening is the signature of coupling between the bright and dark exciton states due to the Aharonov-Bohm effect. Indeed, a magnetic field applied along the SWCNT axis leads to an increase of the energy splitting between these excitonic states and to a transfer of oscillator strength from the bright exciton to the dark. A simple two-level model is used to describe the dependence on applied magnetic field B of the energy splitting $\Delta(B) = [\Delta_0^2 + (wB)^2]^{1/2}$, where Δ_0 is the zero-field energy splitting and w is a constant which depends on the field orientation, the SWCNT diameter, and its chirality [18]. As an example, this evolution provides $\Delta_0 = 5.7$ meV for the (7,6) SWCNT shown in Fig. 1(d).

High-quality PL spectra recorded over long integration times enable the investigation of the finest spectral features. As exemplified in Fig. 1(e) for a (6,5) SWCNT, a low-energy line is evidenced in zero magnetic field, with an intensity representing about 1% of the total PL intensity. Its separation from the bright exciton recombination line coincides with Δ_0 for all investigated SWCNTs [see the inset of Fig. 1(e)]. Therefore, we assign this feature to the zero-field residual dark exciton radiative recombination. This dark state brightening is attributed to a zero-field Aharonov-Bohm effect due to an intrinsic spin-orbit coupling in carbon nanotubes induced by their curvature [19–22], although symmetry breaking by the presence of magnetic impurities [7,23] or static strain effects [24] cannot be completely ruled out. The spin-orbit coupling is due to the σ-π orbital hybridization of the covalent bonds resulting from folding the graphene sheet to a nanotube and is equivalent to the presence of an Aharonov-Bohm magnetic flux $\phi_{SO} = 2\delta p \phi_0$ passing through the nanotube cross section [19], where ϕ_0 is the flux quantum. The dimensionless parameters δ and p are directly related to the strength of the spin-orbit interaction and transfer integrals for σ and π orbitals and have been estimated to be of the order of 10^{-2}–10^{-3} and 0.05, respectively [19]. Over four chiralities, we find an effective magnetic flux $\phi_{SO} \sim 10^{-4}\phi_0$ in zero field, which is consistent with the theoretical [19] and experimental [24,25] estimations.

The magnetic field dependence of the PL spectra is now combined with the investigation of the PL decay of the same single SWCNTs. Figure 2(a) shows the PL decay of the (7,6) SWCNT whose spectra are displayed in Fig. 1(d), for various applied magnetic fields. The decay is biexponential with a short component within few tens of picoseconds, which lies within the temporal resolution of our single-photon-counting system and thus can hardly be exploited. The weight of the long decay component, which is negligible at zero field, drastically increases with magnetic field, while its characteristic time shortens from 1 ns at 0 T to 0.2 ns at 7 T. This behavior, common to all studied SWCNTs, is a signature of the Aharonov-Bohm bright-dark mixing. We model it with a simple two-level system taking into account the bright and dark excitons, with zero-field recombination rates Γ_b and Γ_d and populations p_b and $1 - p_b$ just after photoexcitation of higher-energy exciton states, respectively [see Fig. 2(b)]. Since the bright-dark splitting is at least one order of magnitude larger than the thermal energy k_BT, phonon-assisted transitions between sublevels are essentially a downhill relaxation [16,26,27] with rate γ. In zero magnetic field, the energy sublevels are associated with the genuine

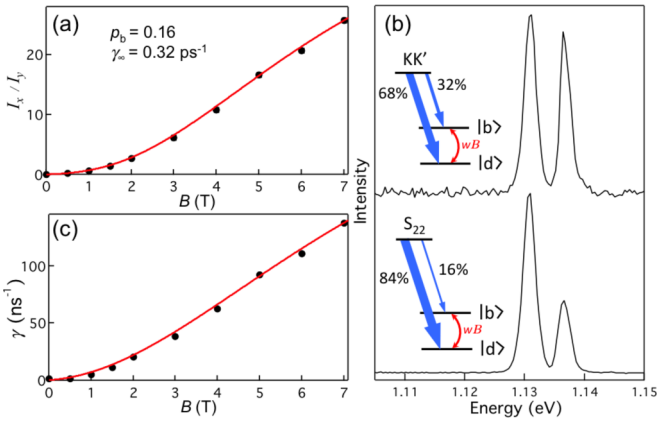

FIG. 3. (a) PL intensity ratio of dark and bright exciton lines as a function of applied magnetic field for a (7,6) SWCNT excited on its S_{22} transition. The red curve is a fit yielding $p_b = 0.16$ and $\gamma_\infty = 0.32$ ps^{-1}, taking $\Delta_0 = 5.7$ meV, $w = 0.68$ meV T^{-1}, $B_{\text{eff}} = 0.28$ T, $\Gamma_d = 1.1$ ns^{-1}, and $\Gamma_b = 20$ ns^{-1} from Figs. 1 and 2. (b) PL spectra of the same nanotube at 2 T for KK' and for S_{22} excitation. The schemes indicate the distribution of populations among bright and dark states in zero field. (c) Bright-to-dark relaxation rate deduced from I_x/I_y for different fields, taking $p_b = 0.16$. The red curve is a plot of $\gamma(B)$ with $\gamma_\infty = 0.32$ ps^{-1}, taking $\Delta_0 = 5.7$ meV, $w = 0.68$ meV T^{-1}, and $B_{\text{eff}} = 0.28$ T.

bright and dark states having odd parity and even parity [7,28], respectively. Thus, phonon-assisted transitions between them are forbidden. However, Aharonov-Bohm mixing of the bright state $|b\rangle$ and the dark state $|d\rangle$ leads to the eigenstates $|x\rangle = \alpha|d\rangle - \beta|b\rangle$ and $|y\rangle = \beta|d\rangle + \alpha|b\rangle$, where $\alpha^2 = (\Delta + \Delta_0)/2\Delta$ and $\beta^2 = (\Delta - \Delta_0)/2\Delta$, and will therefore foster phonon-assisted relaxation between the energy sublevels. This rate is given by $\gamma(B) = 4\gamma_\infty|\alpha(B_{\text{eff}})\beta(B_{\text{eff}})|^2 = \gamma_\infty[wB_{\text{eff}}/\Delta(B_{\text{eff}})]^2$, where $B_{\text{eff}} = B + B_{\text{SO}}$ is the sum of the applied field B and the field B_{SO} associated with the magnetic flux ϕ_{SO} due to spin-orbit coupling. In the limit of high magnetic field the rate is γ_∞, while in zero field $\gamma(0)$ is much smaller than Γ_b [26,27]. Using rate equations to derive the population dynamics of the dark and bright excitons after pulsed excitation, the long component relaxation rate has a magnetic field dependence given by $\Gamma_L = (\Gamma_b + \Gamma_d)/2 - (\Gamma_b - \Gamma_d)\Delta_0/2\Delta$ at zero temperature. Figure 2(c) shows Γ_L as a function of Δ_0/Δ for the same (7,6) SWCNT. This evolution follows the expected linear behavior and enables the derivation of $\Gamma_d = 1.1$ ns^{-1}, and $\Gamma_b = 20$ ns^{-1} which is consistent with the zero-field decay rate of the short component.

The determination of the dark and bright exciton recombination rates enables further derivation of the key parameters governing the relaxation dynamics of the two-level system, namely, $\gamma(B)$ and p_b. Besides the energy splitting between excitons, the PL spectra unveil the evolution with magnetic field of the PL intensity ratio I_x/I_y of the $|x\rangle$ and $|y\rangle$ recombination lines, as shown in Fig. 3(a) for the same (7,6) SWCNT excited on the S_{22} transition. The stationary populations of the two-level model leads to $I_x/I_y = [(1 - p_y)\Gamma_y + \gamma]\beta^2/p_y\Gamma_x\alpha^2$, where $p_y = \alpha^2 p_b + \beta^2(1 - p_b)$ is the population of $|y\rangle$ after photoexcitation, and $\Gamma_x = \alpha^2\Gamma_d + \beta^2\Gamma_b$ and $\Gamma_y = \beta^2\Gamma_d + \alpha^2\Gamma_b$ are the recombination rates of $|x\rangle$ and $|y\rangle$, respectively. Fitting the evolution of I_x/I_y with these expressions yields $\gamma_\infty = 0.32$ ps^{-1} and $p_b = 0.16$. For all studied SWCNTS, the value of p_b is remarkably low, ranging from 6% to 30% depending on the chirality. This observation is consistent with a recent terahertz spectroscopic study of ultrafast absorption of the dark-to-bright transition after S_{22} photoexcitation [29] and avoids resorting to previous assumptions of selective population transfer to the bright exciton [16,30] or of equally distributed initial populations of the excitons [27,31] after relaxation from the S_{22} levels. We also performed photoexcitation on the KK' phonon sideband, which produces a significantly larger population of the bright exciton than under S_{22} photoexcitation, as exemplified in Fig. 3(b). Interestingly, Fig. 3(c) displays the values of $\gamma(B)$ deduced for various amplitudes of applied magnetic field. It shows evidence for the drastic enhancement of the relaxation between sublevels due to Aharonov-Bohm symmetry breaking. The upper value γ_∞ reached by the relaxation rate at high dark and bright states mixing approaches the interband relaxation rates [32] of the order of 0.5 ps^{-1}, while for weak fields γ vanishes [26,27] (values within the error bar of 2 ns^{-1}).

We now discuss the width and the shape of the recombination lines in the low-temperature PL spectra of single SWCNTs. In previous works, a variety of line shapes have been observed for the bright exciton [33–38], from narrow lines in suspended nanotubes to broad and asymmetrical line shapes with low-energy wings. The redshifted wings have been modeled and attributed to radiative recombination of a spatially confined exciton assisted by the emission of phonons from a unidimensional acoustic phonon bath [36]. It has been proposed that the diversity of the low-temperature PL profiles of single SWCNTs stems from tiny modifications in their density of low-energy acoustic phonon modes [38]. The high-quality PL spectra recorded in this Rapid Communication reveal interesting features in the PL line shapes. First, for all chiralities, bright exciton lines are narrower than that of the dark exciton, as exemplified in Fig. 1. The contribution of exciton population relaxations to the homogenous linewidths being negligible, the main mechanism of homogeneous broadening is pure dephasing of the transition dipole due to the coupling of the exciton to acoustic phonon modes [39–42]. Since the effective mass of the dark exciton is larger than that of the bright by an order of magnitude [7], our observations suggest that the dephasing rate depends on the effective mass m^* of the exciton, in qualitative agreement with theoretical models which predict a phonon scattering rate proportional to $\sqrt{m^*}$ [32,43]. This assertion is further supported by a close examination of the PL spectra in Figs. 4(a) and 4(b), where the bright exciton line broadens with magnetic field, while that of the dark exciton sharpens. This behavior can be explained by the evolution of the dispersions of the bright and dark excitons with magnetic field [18]. Indeed, the Aharonov-Bohm coupling leads to an increase in effective mass for the initially bright level and a decrease for the initially dark level, as illustrated in Fig. 4(c). Second, a striking asymmetry of the bright exciton recombination line is found for all studied single SWCNTs, as exemplified in Figs. 1 and 4(d). The bright exciton line presents a high-energy wing with respect to the zero-phonon line (ZPL), in stark contrast with the usual

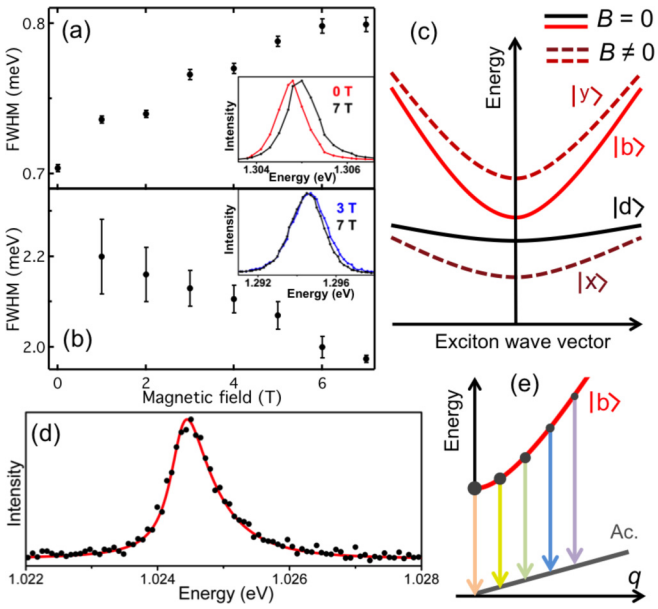

FIG. 4. Evolution of the (a) bright and (b) dark exciton recombination linewidths of a (6,5) SWCNT with increasing magnetic fields. Some PL spectra are displayed in the insets. (c) Illustration of the dispersions for the bright and dark exciton bands in zero field (plain curves) and the mixed excitons at high magnetic field (dashed curves). (d) Asymmetry of the bright exciton recombination line. The red curve is a simulation of the line profile with Eq. (1), using $\Gamma = 0.5$ meV and a ZPL weight of 25%. (e) Scheme of the dispersions for the bright exciton band and an acoustic phonon branch. The arrows indicate phonon-assisted excitonic transitions.

low-energy phonon sidebands observed in the PL line shapes of localized nanotube excitons [36,38]. We interpret these line shapes as a signature of the free nature of excitons in these SWCNTs. In addition to the recombination of the zero-momentum exciton (on the ZPL), radiative recombination of the exciton with q momentum occurs with the emission or absorption of an acoustic phonon carrying the same momentum. The spectral distribution of the phonon wings depends both on exciton and phonon dispersion relations to fulfill energy and momentum conservation, as illustrated in Fig. 4(e). For simplicity, we consider a single acoustic phonon branch of velocity c_s. A blueshifted acoustic phonon sideband will develop in the case of the bright exciton due to its steep, nonparabolic dispersion relation varying as $E_{\rm ex}(q) = E^0_{\rm ex} + Aq^2 \log(q_0/|q|)$ [7,31], where q is the exciton wave vector, $E^0_{\rm ex}$ the band-edge exciton energy, q_0 a momentum cutoff, and A a coupling constant that measures the strength of the exchange energy. Assuming that intraband thermalization is much faster than the recombination dynamics [44], we consider a Maxwell-Boltzmann distribution of the exciton momenta in the bright band. The phonon sideband intensity at the photon energy E is obtained by summing the weighted Lorentzian contributions of all possible q-momenta excitons to the emission, taking into account the phonon population,

$$I_{\rm PS}(E) \propto \int \left\{ \frac{|g_q^{Ac}|^2}{[E + \hbar c_s q - E_{\rm ex}(q)]^2 + \frac{\Gamma^2}{4}} (N_B + 1) + \frac{|g_q^{Ac}|^2}{\left[E - \hbar c_s q - E_{\rm ex}(q)\right]^2 + \frac{\Gamma^2}{4}} N_B \right\} \times \exp\left[-\frac{E_{\rm ex}(q) - E^0_{\rm ex}}{k_B T} \right] dq, \quad (1)$$

where $N_B = 1/[\exp(\hbar c_s q/k_B T) - 1]$, $|g_q^{Ac}|^2 \propto q$ is the squared matrix element of the exciton-phonon coupling [44], and $\Gamma/\hbar$ is the dephasing rate. The first (second) term of this expression corresponds to the process of phonon emission (absorption) involved in the exciton recombination. To reproduce the PL profile, a Lorentzian ZPL of width Γ is added to this phonon sideband with an adjustable relative scaling parameter. The simulations in Fig. 4(d) are performed with $c_s = 20$ km s^{-1} [43,45,46], $A = 2.85$ eV nm^2, $q_0 = 1.4$ nm^{-1} [31], and reproduce well the experimental spectra.

Finally, the assumption of free excitons is supported by the absence of a trion fingerprint in the PL spectra recorded under strong excitation intensities. Indeed, for single SWCNTs immobilized in agarose gels or spin coated on surfaces, trions can be formed at high laser powers due to Auger photogeneration of free charges that subsequently trap in the electrostatic potential fluctuations along the nanotube [47]. The systematic high-energy wing observed in the bright exciton recombination line shape is thus attributed to a unique signature of the free character of the exciton and points to a drastic reduction of environmental perturbations of these high-quality suspended nanotubes.

We thank Jonah Shaver for his participation at the early stage of the work, and Naoto Akizuki for preparation of samples. We acknowledge the financial support from Idex Bordeaux (LAPHIA Program) and the Institut Universitaire de France. B.L. is grateful to the Japan Society for the Promotion of Science for support through a fellowship.

[1] M. J. O'Connell, S. M. Bachilo, C. B. Huffman, V. C. Moore, M. S. Strano, E. H. Haroz, K. L. Rialon, P. J. Boul, W. H. Noon, C. Kittrell, J. Ma, R. H. Hauge, R. B. Weisman, and R. E. Smalley, Science **297**, 593 (2002).

[2] S. M. Bachilo, M. S. Strano, C. Kittrell, R. H. Hauge, R. E. Smalley, and R. B. Weisman, Science **298**, 2361 (2002).

[3] P. Avouris, M. Freitag, and V. Perebeinos, Nat. Photonics **2**, 341 (2008).

[4] F. Wang, G. Dukovic, L. E. Brus, and T. F. Heinz, Science **308**, 838 (2005).

[5] J. Maultzsch, R. Pomraenke, S. Reich, E. Chang, D. Prezzi, A. Ruini, E. Molinari, M. S. Strano, C. Thomsen, and C. Lienau, Phys. Rev. B **72**, 241402(R) (2005).

[6] C. D. Spataru, S. Ismail-Beigi, R. B. Capaz, and S. G. Louie, Phys. Rev. Lett. **95**, 247402 (2005).

[7] V. Perebeinos, J. Tersoff, and P. Avouris, Nano Lett. **5**, 2495 (2005).

[8] T. Ando, J. Phys. Soc. Jpn. **75**, 024707 (2006).
[9] O. N. Torrens, M. Zheng, and J. M. Kikkawa, Phys. Rev. Lett. **101**, 157401 (2008).
[10] A. Srivastava, H. Htoon, V. I. Klimov, and J. Kono, Phys. Rev. Lett. **101**, 087402 (2008).
[11] H. Ajiki and T. Ando, J. Phys. Soc. Jpn. **62**, 2470 (1993).
[12] H. Ajiki, J. Phys.: Condens. Matter **24**, 483001 (2012).
[13] S. Zaric, G. N. Ostojic, J. Kono, J. Shaver, V. C. Moore, M. S. Strano, R. H. Hauge, R. E. Smalley, and X. Wei, Science **304**, 1129 (2004).
[14] S. Zaric, G. N. Ostojic, J. Shaver, J. Kono, O. Portugall, P. H. Frings, G. L. J. A. Rikken, M. Furis, S. A. Crooker, X. Wei, V. C. Moore, R. H. Hauge, and R. E. Smalley, Phys. Rev. Lett. **96**, 016406 (2006).
[15] R. Matsunaga, K. Matsuda, and Y. Kanemitsu, Phys. Rev. Lett. **101**, 147404 (2008).
[16] R. Matsunaga, Y. Miyauchi, K. Matsuda, and Y. Kanemitsu, Phys. Rev. B **80**, 115436 (2009).
[17] S. Maruyama, R. Kojima, Y. Miyauchi, S. Chiashi, and M. Kohno, Chem. Phys. Lett. **360**, 229 (2002).
[18] J. Shaver, J. Kono, O. Portugall, V. Krstić, G. L. J. A. Rikken, Y. Miyauchi, S. Maruyama, and V. Perebeinos, Nano Lett. **7**, 1851 (2007).
[19] T. Ando, J. Phys. Soc. Jpn. **69**, 1757 (2000).
[20] L. Chico, M. P. López-Sancho, and M. C. Muñoz, Phys. Rev. B **79**, 235423 (2009).
[21] W. Izumida, K. Sato, and R. Saito, J. Phys. Soc. Jpn. **78**, 074707 (2009).
[22] H. Liu, D. Heinze, H. T. Duc, S. Schumacher, and T. Meier, J. Phys.: Condens. Matter **27**, 445501 (2015).
[23] J. Shaver and J. Kono, Laser Photonics Rev. **1**, 260 (2007).
[24] A. Nish, R. J. Nicholas, C. Faugeras, Z. Bao, and M. Potemski, Phys. Rev. B **78**, 245413 (2008).
[25] F. Kuemmeth, S. Ilani, D. C. Ralph, and P. L. McEuen, Nature (London) **452**, 448 (2008).
[26] S. Berciaud, L. Cognet, and B. Lounis, Phys. Rev. Lett. **101**, 077402 (2008).
[27] T. Gokus, L. Cognet, J. G. Duque, M. Pasquali, A. Hartschuh, and B. Lounis, J. Phys. Chem. C **114**, 14025 (2010).
[28] V. Perebeinos, J. Tersoff, and P. Avouris, Phys. Rev. Lett. **94**, 027402 (2005).
[29] L. Luo, I. Chatzakis, A. Patz, and J. Wang, Phys. Rev. Lett. **114**, 107402 (2015).
[30] T. Nishihara, Y. Yamada, and Y. Kanemitsu, Phys. Rev. B **86**, 075449 (2012).
[31] J. J. Crochet, J. G. Duque, J. H. Werner, B. Lounis, L. Cognet, and S. K. Doorn, Nano Lett. **12**, 5091 (2012).
[32] V. N. Popov and P. Lambin, Phys. Rev. B **74**, 075415 (2006).
[33] J. Lefebvre, J. M. Fraser, P. Finnie, and Y. Homma, Phys. Rev. B **69**, 075403 (2004).
[34] H. Htoon, M. J. O'Connell, P. J. Cox, S. K. Doorn, and V. I. Klimov, Phys. Rev. Lett. **93**, 027401 (2004).
[35] K. Matsuda, T. Inoue, Y. Murakami, S. Maruyama, and Y. Kanemitsu, Phys. Rev. B **77**, 033406 (2008).
[36] C. Galland, A. Högele, H. E. Türeci, and A. Imamoğlu, Phys. Rev. Lett. **101**, 067402 (2008).
[37] I. Sarpkaya, Z. Zhang, W. Walden-Newman, X. Wang, J. Hone, C. W. Wong, and S. Strauf, Nat. Commun. **4**, 2152 (2013).
[38] F. Vialla, Y. Chassagneux, R. Ferreira, C. Roquelet, C. Diederichs, G. Cassabois, P. Roussignol, J. S. Lauret, and C. Voisin, Phys. Rev. Lett. **113**, 057402 (2014).
[39] Y.-Z. Ma, M. W. Graham, G. R. Fleming, A. A. Green, and M. C. Hersam, Phys. Rev. Lett. **101**, 217402 (2008).
[40] K. Yoshikawa, R. Matsunaga, K. Matsuda, and Y. Kanemitsu, Appl. Phys. Lett. **94**, 093109 (2009).
[41] D. Karaiskaj and A. Mascarenhas, Phys. Rev. B **75**, 115426 (2007).
[42] D. T. Nguyen, C. Voisin, P. Roussignol, C. Roquelet, J. S. Lauret, and G. Cassabois, Phys. Rev. B **84**, 115463 (2011).
[43] G. Pennington and N. Goldsman, Phys. Rev. B **71**, 205318 (2005).
[44] C. Köhler, T. Watermann, and E. Malic, J. Phys.: Condens. Matter **25**, 105301 (2013).
[45] R. Saito, G. Dresselhaus, and M. S. Dresselhaus, *Physical Properties of Carbon Nanotubes* (Imperial College Press, London, 1998).
[46] J. Hone, in *Carbon Nanotubes*, edited by M. S. Dresselhaus, G. Dresselhaus, and P. Avouris (Springer, Berlin, 2001), pp. 273–286.
[47] S. M. Santos, B. Yuma, S. Berciaud, J. Shaver, M. Gallart, P. Gilliot, L. Cognet, and B. Lounis, Phys. Rev. Lett. **107**, 187401 (2011).